Materials Advances

ROYAL SOCIETY OF CHEMISTRY

PAPER

View Article Online
View Journal | View Issue

Cite this: *Mater. Adv.*, 2022, 3, 1047

Tuning ionic conductivity to enable all-climate solid-state Li–S batteries with superior performances†

Chaochao Wei,[ab] Chuang Yu,*[a] Linfeng Peng,[a] Ziqi Zhang,[c] Ruonan Xu,[c] Zhongkai Wu,[a] Cong Liao,[a] Wei Zhang,[a] Long Zhang,[c] Shijie Cheng[a] and Jia Xie*[a]

Low Li-ion mobility of the cathode mixture is one of the major obstacles for Li_2S-based solid-state Li–S achieving excellent electrochemical performances. The poor Li-ion conductivity is due to the intrinsic insulation of Li_2S and the low Li-ion mitigation across the Li_2S/solid electrolyte interface. Here, we propose the correlation between the increased Li-ion conductivity of the cathode mixture and electrochemical performances of solid-state batteries using Li_2S as an active material. Replacing Li_6PS_5Cl with a superior conductive $Li_{5.5}PS_{4.5}Cl_{1.5}$ solid electrolyte increases the interfacial ionic mobility and reduces the solid/solid resistance, resulting in higher discharge capacities and better cycling performances. In addition, the Li-ion conductivity of Li_2S is enhanced by reducing the particle sizes using high-rotation milling, and a further improvement is achieved by mixing the obtained milled Li_2S with LiI. The $3Li_2S$–LiI cathode mixture with high room temperature ionic conductivity and a comparable Li_2S loading amount is chosen as the cathode and combined with the $Li_{5.5}PS_{4.5}Cl_{1.5}$ solid electrolyte to fabricate solid-state Li–S batteries. The assembled battery displays excellent electrochemical performances at different operating temperatures. Our findings in this work could help to promote the development of Li_2S-based solid-state Li–S batteries.

Received 23rd October 2021,
Accepted 17th November 2021

DOI: 10.1039/d1ma00987g

rsc.li/materials-advances

Introduction

With the development of electric vehicles and portable electronics, the demand for high energy density batteries becomes urgent.[1–3] Lithium–sulfur (Li–S) batteries have attracted great attention due to the high theoretical specific capacity of sulfur (~1675 mA h g^{-1}).[4–10] However, during the charge and discharge processes, the S cathode quickly generates polysulfides that are soluble in the liquid electrolyte, forming a shuttle effect between the cathode and anode, resulting in low coulombic efficiency and short span life of lithium–sulfur batteries.[11–14] Replacing the liquid electrolyte with the solid electrolyte to fabricate solid-state batteries can physically block polysulfides, avoid the shuttle effect, and improve the safety and energy density.[15–17] However, sulfur suffers large volume changes and low electronic conductivity.[18,19] In contrast, Li_2S with comparable theoretical capacity, smaller stress changes, better thermal stability, and much higher electronic conductivity than sulfur shows significant potential as a cathode material for Li–S batteries.[20–22] Moreover, the Li_2S cathode provides the possibility of utilizing lithium-free anodes.

The major hindrance for Li_2S-based solid-state batteries to achieve high electrochemical performances is the slow electronic/ionic kinetics of electrodes. Therefore, tuning the cathode component with a fast three-dimensional conductive framework is vital to construct solid-state batteries. Unlike the fluidity liquid electrolyte that can infiltrate the active material, solid electrolytes need to be introduced in the electrode mixture to enhance the ionic conductivity.[23] Hence, improving the ionic conductivity of the Li_2S cathode mixture can effectively increase the kinetics. Besides, the ionically insulating Li_2S also lowers the battery performance. Our previous research has reported that the ionic conductivity of Li_2S increased *via* reducing the particle size due to the short diffusion distance.[24] Lin *et al.*[25] prepared nano-sized Li_2S with a liquid route and delivered a high discharge specific capacity of 848 mA h g^{-1} at 0.1C at 60 °C. Moreover, it has been reported that the ionic

[a] State Key Laboratory of Advanced Electromagnetic Engineering and Technology, School of Electrical and Electronic Engineering, Huazhong University of Science and Technology, Wuhan 430074, P. R. China. E-mail: cyu2020@hust.edu.cn, xiejia@hust.edu.cn
[b] School of Chemistry and Chemical Engineering, Huazhong University of Science and Technology, Wuhan 430074, P. R. China
[c] Clean Nano Energy Center, State Key Laboratory of Metastable Materials Science and Technology, Yanshan University, Qinhuangdao 066004, China

† Electronic supplementary information (ESI) available. See DOI: 10.1039/d1ma00987g

conductivity of Li_2S can be enhanced *via* the introduction of LiX (X = Cl, Br). The ionic conductivity of Li_2S increased after mixing with LiI and the corresponding electrode showed a high initial discharge capacity of 663 mA h g^{-1}.[26] Furthermore, introducing LiI in a solid-state battery can both improve the tolerance of sulfide towards the lithium metal and enhance the lithium dissolution/deposition during cycling.[27] Although the introduction of LiX (X = Cl, Br) can yield fast lithium mobility, LiX can hardly act as an active material to provide capacity.[28] As a result, the energy density of the fabricated solid-state battery using the above electrode decreases due to the increasing amount of LiX. Optimizing the weight ratio of LiX in the Li_2S–LiX electrode can balance the ionic kinetic and effective active material, yielding a suitable electrode with excellent electrochemical and high energy density.

Solid electrolytes work as a combination of a liquid electrolyte and a separator in solid-state batteries,[29,30] the ionic conductivities of which play a vital role in electrochemical performance.[31,32] In typical inorganic conductors, the ionic conductivities of solid electrolytes highly depend on operating temperatures.[33,34] Moreover, the ionic kinetics and interfacial contact of solid–solid are influenced by the ambient temperature. Therefore, unraveling the working mechanism and electrochemical performances of Li_2S-based solid-state batteries at various temperatures is helpful to promote its application.

In this work, to construct Li_2S-based solid-state Li–S batteries with high energy density, we need to optimize both the solid-state electrolyte and the Li_2S active material. First, the solid electrolyte $Li_{5.5}PS_{4.5}Cl_{1.5}$ with a high ionic conductivity (8×10^{-3} S cm^{-1}) was used to increase the ionic dynamics and improve the electrochemical performance of the battery. Second, a series of $x$$Li_2S$–LiI electrode mixtures were obtained by ball milling to improve the ionic insulation of the active material itself. As expected, the prepared all-solid-state battery has high discharge capacity, excellent cycle stability and excellent rate performance. The mechanism of all-solid-state batteries with these excellent electrochemical properties was studied. In addition, the working mechanism and electrochemical properties of all-solid-state batteries at high and low temperatures were also studied.

Experimental section

Preparation of M-Li_2S and $x$$Li_2S$–LiI

Reagent-grade Li_2S (Sigma-Aldrich, 99.9%) powder was placed into a ZrO_2-coated stainless steel pot with ZrO_2 balls. It was then mechanically milled with a planetary ball mill (Fritsch Pulverisette 7) for 20 h at 510 rpm. Finally, M-Li_2S (milled-Li_2S) was obtained. M-Li_2S obtained by previous ball milling and reagent-grade LiI (Sigma-Aldrich, 99.9%) powders were mixed with the required amount ratio using a ZrO_2-coated stainless steel pot with ZrO_2 balls. The mixture was first ball milled with a rotation speed of 110 rpm for 2 h and then mechanically milled for 4 h at 500 rpm to obtain a series of $x$$Li_2S$–LiI ($x$ = 3, 5, 7, 9).

Preparation of Li_6PS_5Cl and $Li_{5.5}PS_{4.5}Cl_{1.5}$ solid electrolytes

Reagent-grade Li_2S (Sigma-Aldrich, 99.9%), P_2S_5 (Macklin, 99%) and LiCl (Sigma-Aldrich, 99.9%) powders were mixed with the required amount ratio using a ZrO_2-coated stainless steel pot with ZrO_2 balls. The total weight ratios of ZrO_2 balls and the mixture of raw materials were fixed at 20/1. The total amount of the starting materials was 2.0 g for each pot. The mixture was first ball milled with a rotation speed of 110 rpm for 1 h and then was sealed in a quartz tube and annealed at 500 °C for 15 h.

Preparation of composite electrodes

The composite electrodes consist of Li_2S based active materials, a solid electrolyte (SE) and conductive carbon black (KB-800) in a weight ratio of 4 : 4 : 2. The mixture was first ball milled with a rotation speed of 110 rpm for 30 min and then mechanically milled for 4 h at 500 rpm. The obtained composite electrode powders were used as working electrodes in all-solid-state cells.

Material characterization

X-ray diffraction (XRD, 2θ = 10°–80°, Rigaku MiniFlex600/600-c) with Cu-Kα radiation was used to observe the structure. Lithium-ion conductivities of the solid electrolytes were characterized by pelletizing 100 mg powder into a pellet (diameter of 10 mm) using stainless steel as the blocking electrodes. The alternating current (AC) impedance spectrum was recorded using an impedance analyzer (Solartron, 1260) in the frequency range of 1 Hz to 7 MHz with an applied voltage of 0.02 V. The morphology and energy-dispersive spectroscopy (EDS) mapping of the solid electrolytes and the composite electrodes were observed by scanning electron microscopy (SEM, FEI FIB Helios G).

The fabrication and electrochemical measurements of all-solid-state Li–S batteries

For assembling the Li_2S/Li_6PS_5Cl/In–Li cell, 80 mg Li_6PS_5Cl was pelleted first as the solid electrolyte layer, and then 5 mg above cathode mixture (Li_2S : Li_6PS_5Cl solid electrolyte : conductive carbon black = 4 : 4 : 2) was evenly spread and pressed at 380 MPa. The Li–In alloy was employed as the anode electrode and pressed at 150 MPa. To fabricate $x$$Li_2S$–LiI/$Li_{5.5}PS_{4.5}Cl_{1.5}$/In–Li cells, the operation steps are the same as above, and the solid electrolyte is replaced by $Li_{5.5}PS_{4.5}Cl_{1.5}$, the cathode is replaced by the mixture of $x$$Li_2S$–LiI, $Li_{5.5}PS_{4.5}Cl_{1.5}$ solid electrolyte, and carbon black with a weight ratio of 4 : 4 : 2. Galvanostatic charge–discharge cycling tests were performed using a multi-channel battery test system (LAND CT2001A) and (Neware CT-ZWJ-4s-T-1U) between 0.4 and 3 V at 0 °C, 25 °C (RT), and 60 °C.

Results and discussion

The XRD pattern in Fig. S1 (ESI†) confirms that pure Li_6PS_5Cl with a cubic structure has been successfully synthesized. The impedance results show a Li-ion conductivity of 1.1 mS cm^{-1} for the obtained Li_6PS_5Cl electrolyte, as shown in Fig. 1a.

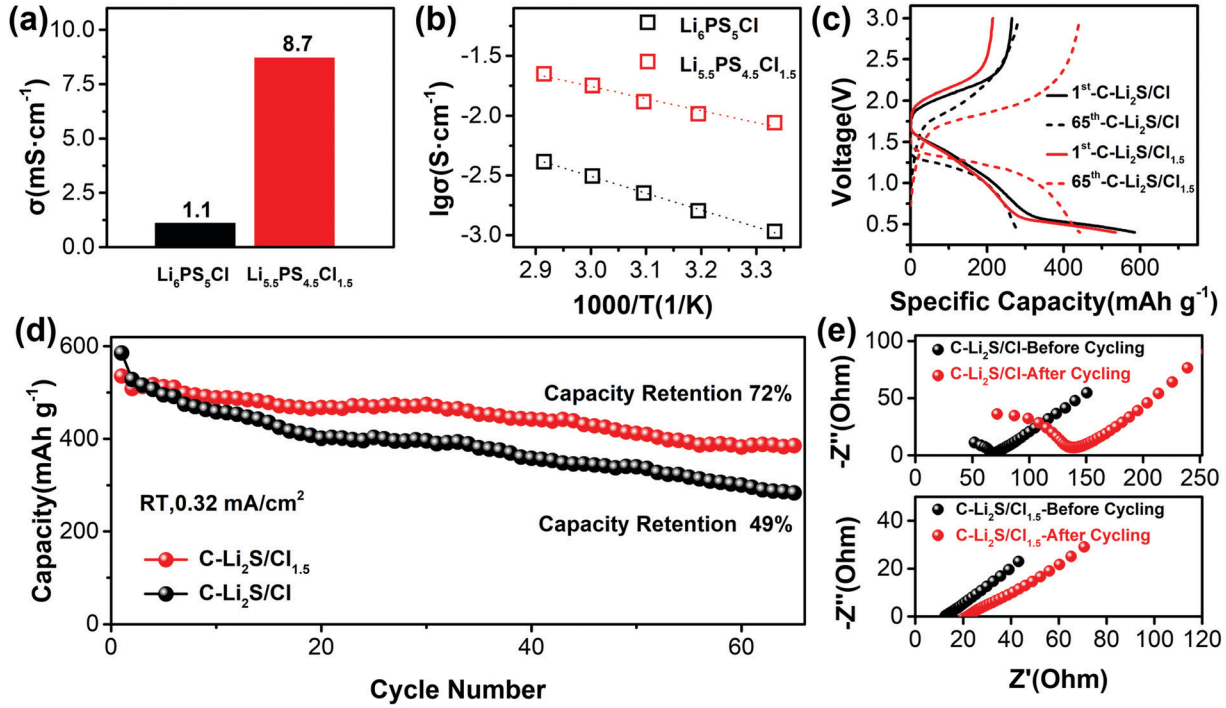

Fig. 1 (a) The ionic conductivity of Li_6PS_5Cl and $Li_{5.5}PS_{4.5}Cl_{1.5}$ solid electrolytes measured at room temperature. (b) The corresponding Arrhenius plots of ionic conductivities at different temperatures. (c) Initial and after 65th cycling charge/discharge curves of C-Li_2S/Li_6PS_5Cl/In–Li and C-Li_2S/$Li_{5.5}PS_{4.5}Cl_{1.5}$/In–Li solid-state batteries cycled at 0.32 mA cm^{-2} between 0.4 and 3 V *vs.* Li–In at room temperature. (d) Cycling performances of these assembled solid-state batteries. (e) EIS of these two batteries before and after 65 cycles at room temperature.

Previous research found that enriching halogen in the structure of Li_6PS_5X (X = Cl, Br) electrolytes can significantly enhance their Li-ion conductivities.[27] Hence, $Li_{5.5}PS_{4.5}Cl_{1.5}$ with a room temperature conductivity of 8.7 mS cm^{-1}, almost seven times higher than that of the Li_6PS_5Cl electrolyte (Fig. 1a), was prepared using the simple solid-state reaction method. Moreover, according to the impedance results (Fig. S2, ESI†), the former delivers much higher Li-ion conductivities than the latter at different measuring temperatures, as shown in Fig. 1b. To investigate the influence of Li-ion conductivities of solid electrolytes on the electrochemical performances, solid-state Li–S batteries using Li_6PS_5Cl and $Li_{5.5}PS_{4.5}Cl_{1.5}$ electrolytes combined with the commercial Li_2S (C-Li_2S) cathode and the Li–In anode were fabricated and cycled at 0.32 mA cm^{-2} between 0.4 and 3.0 V *vs.* Li–In at room temperature. In Fig. 1c, these assembled batteries deliver comparable discharge capacities at this current density for the 1st cycle. After 65 cycles, C-Li_2S/Li_6PS_5Cl/Li–In sustains a discharge capacity of 283 mA h g^{-1} with a capacity retention of 49% (Fig. 1d). In contrast, C-Li_2S/$Li_{5.5}PS_{4.5}Cl_{1.5}$/Li–In achieves a much higher capacity of 385 mA h g^{-1} and a superior capacity retention of 72% under the same measuring conditions. The EIS results before and after cycling confirm that the battery using the Li_6PS_5Cl electrolyte shows a significant increase of the interfacial resistance after 65 cycles than that using the $Li_{5.5}PS_{4.5}Cl_{1.5}$ solid electrolyte (Fig. 1e). Therefore, the utilization of high conductive solid electrolytes for solid-state Li–S batteries provides lower interfacial resistance and fast Li-ion mobility across the active materials/solid electrolyte interfaces. The higher discharge capacities and superior cycling performances of solid-state batteries using $Li_{5.5}PS_{4.5}Cl_{1.5}$ are attributed to the boosting Li-ion conductivity.

The ionic conductivity of active materials also plays a crucial role in the electrochemical performance of solid-state Li–S batteries. A similar strategy of enhancing the ionic conductivity of the Li_2S cathode can be utilized to improve the battery performance. Reducing the particle size of Li_2S has been proved as an effective route to improve capacities and cyclability.[24] C-Li_2S was milled at 550 rpm for 4 h to decrease the particle size and the obtained Li_2S was denoted as M-Li_2S. M-Li_2S shows broader XRD diffraction peaks than C-Li_2S, as shown in Fig. 2a, indicating a smaller particle size. Moreover, SEM images verify that M-Li_2S possesses smaller particle sizes than C-Li_2S after the mechanical milling procedure (Fig. 2b). In Fig. 2c, M-Li_2S delivers much higher Li-ion conductivities than C-Li_2S at different operating temperatures, indicating that the ionic conductivity of Li_2S has been successfully increased *via* lowering the particle size (the conductivity of C-Li_2S at 30 °C and 40 °C cannot be measured due to the frequency limitation of the equipment), and the corresponding activation energy has also been reduced. Fig. 2d depicts the initial charge/discharge curves of M-Li_2S/$Li_{5.5}PS_{4.5}Cl_{1.5}$/Li–In cycled at 0.32 mA cm^{-2} between 0.4 and 3.0 V *vs.* Li–In. It delivers an initial discharge capacity of 556 mA h g^{-1}, which is higher than that of the C-Li_2S/$Li_{5.5}PS_{4.5}Cl_{1.5}$/Li–In batteries described in the above section. In addition, it sustains 458 mA h g^{-1} after 65 cycles, with a

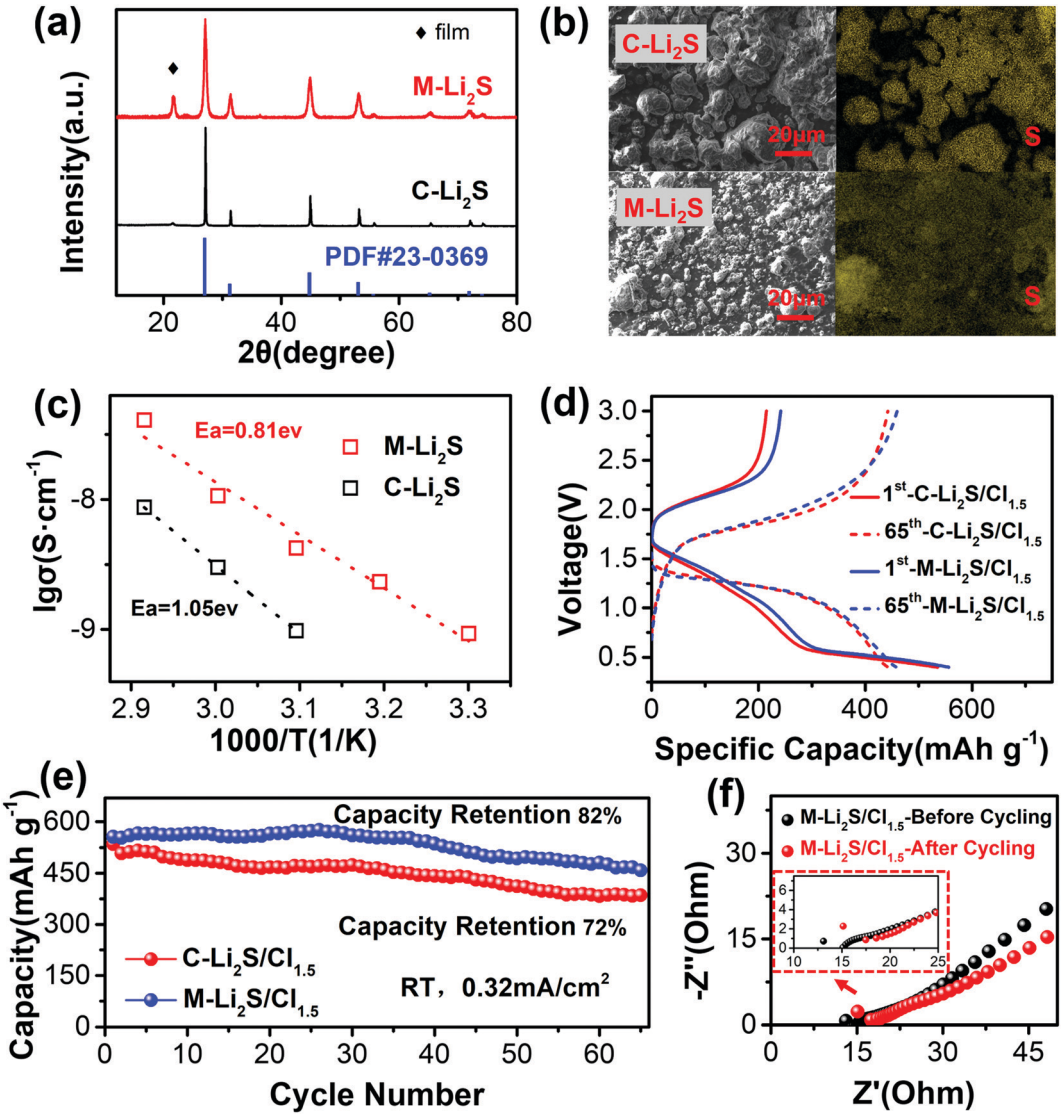

Fig. 2 (a) XRD patterns of C-Li_2S and M-Li_2S. (b) SEM images and EDS mapping of C-Li_2S and M-Li_2S. (c) The corresponding Arrhenius plots of ionic conductivities measured at different temperatures. (d) The initial and 65th cycling charge/discharge curves of C-Li_2S/$Li_{5.5}PS_{4.5}Cl_{1.5}$/In–Li and M-Li_2S/$Li_{5.5}PS_{4.5}Cl_{1.5}$/In–Li solid-state batteries cycled at 0.32 mA cm^{-2} between 0.4 and 3 V *vs.* Li–In at room temperature. (e) Cycling performance of these two batteries and (f) the corresponding EIS before and after 65 cycles.

capacity retention of 82% (Fig. 2e). Under the same measuring conditions, the larger discharge capacity and higher capacity retention for M-Li_2S/$Li_{5.5}PS_{4.5}Cl_{1.5}$/Li–In imply the effectiveness of enlarging the Li-ion conductivity of Li_2S active materials to improve electrochemical performances. The corresponding EIS results before and after cycling confirm that the battery using M-Li_2S shows a slight increase of the interfacial resistance after 65 cycles (Fig. 2f).

Besides reducing the crystalline size, another possible route to increase the Li-ion conductivity of Li_2S is introducing lithium halide.[26] To achieve higher Li-ion conductivity of active materials, LiI was mixed with M-Li_2S *via* the mechanical milling process. The mole ratios of LiI and M-Li_2S were tailored to obtain composite materials with high ionic conductivity and an acceptable active (Li_2S) loading amount. Fig. 3a shows the XRD patterns of the milled Li_2S–LiI mixtures with different ratios x (x = 3, 5, 7, and 9). At low weight ratios (x = 3 and 5), the diffraction peaks are indexed to Li_2S and LiI phases. In contrast, the reflections assigned to the LiI phase decrease with increasing weight ratios (x = 7 and 9) for the milled samples and almost disappear when x = 9. The minor amount of LiI in the mixture could react with a small amount of Li_2S to form an amorphous sulfide electrolyte[35] and left a large percentage of Li_2S materials, yielding degrading ionic conductivity compared to the mixture with a lower mole ratio. Fig. 3b shows the Li-ion conductivities of the milled Li_2S–LiI mixtures at different temperatures. 3Li_2S–LiI shows the highest ionic conductivity among these mixtures at room temperature. In addition, 5Li_2S–LiI with a higher amount of Li_2S exhibits comparable ionic conductivity (Fig. 3c). SEM and EDX images of 3Li_2S–LiI and

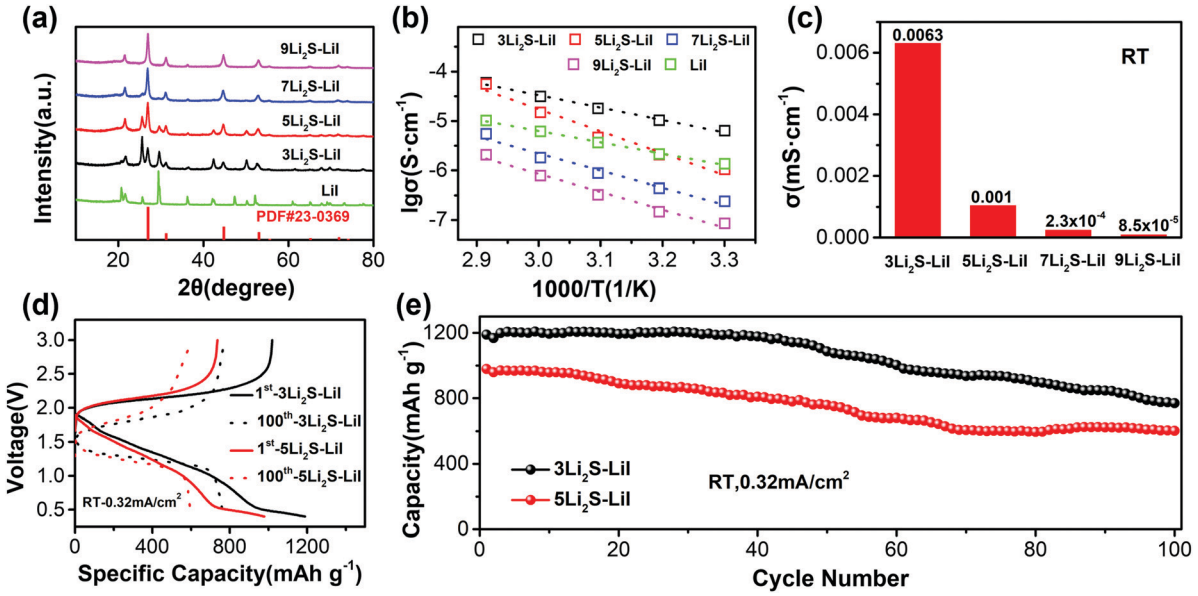

Fig. 3 (a) XRD patterns of Li_2S, LiI, and Li_2S–LiI mixture with different weight ratios. (b) Temperature-dependent Li-ion conductivities of these obtained materials. (c) The ionic conductivity of the Li_2S–LiI mixture measuring at room temperature. (d) Initial and after 100th cycling charge/discharge curves of $Li_{5.5}PS_{4.5}Cl_{1.5}$-based solid-state Li–S batteries using the $3Li_2S$–LiI and $5Li_2S$–LiI cathode mixture cycled at 0.32 mA cm^{-2} between 0.4 and 3 V *vs.* Li–In at room temperature. (e) The corresponding cycling performance.

$5Li_2S$–LiI demonstrate uniform doping and composition of the composite (Fig. S3, ESI†). Therefore, both $3Li_2S$–LiI and $5Li_2S$–LiI were chosen as cathodes to construct solid-state Li–S batteries using $Li_{5.5}PS_{4.5}Cl_{1.5}$ electrolytes with higher Li-ion conductivity. In Fig. 3(d and e), both batteries display similar charge/discharge curves for the 1st and 100th cycles. $3Li_2S$–LiI/$Li_{5.5}PS_{4.5}Cl_{1.5}$/Li–In delivers an initial discharge capacity of 1190 mA h g^{-1}, while $5Li_2S$–LiI/$Li_{5.5}PS_{4.5}Cl_{1.5}$/Li–In shows a smaller discharge capacity of 980 mA h g^{-1} at 0.32 mA cm^{-2} at ambient temperature. These values are much higher than those of the above $Li_{5.5}PS_{4.5}Cl_{1.5}$-based solid-state batteries using C- and M-Li_2S cathodes, indicating that increasing the ionic conductivity of Li_2S active materials can effectively enhance the capacities. After 100 cycles at 0.32 mA cm^{-2}, $3Li_2S$–LiI/$Li_{5.5}PS_{4.5}Cl_{1.5}$/Li–In and $5Li_2S$–LiI/$Li_{5.5}PS_{4.5}Cl_{1.5}$/Li–In batteries still sustain 770 and 600 mA h g^{-1}, with the corresponding capacity retention of 64.7% and 61.2%, respectively.

To reveal the influence of ionic conductivity on the impedance change of solid-state Li–S batteries during cycling, *in situ* EIS of the $3Li_2S$–LiI/$Li_{5.5}PS_{4.5}Cl_{1.5}$/Li–In and $5Li_2S$–LiI/$Li_{5.5}PS_{4.5}Cl_{1.5}$/Li–In solid-state batteries was performed at room temperature. As shown in Fig. 4a, the bulk impedance of the $3Li_2S$–LiI/$Li_{5.5}PS_{4.5}Cl_{1.5}$/Li–In battery increased during the first charging process, and the decomposition of the sulfide solid electrolyte during cycling caused this increase of interfacial resistance.[36] As shown in Fig. 4b, the $5Li_2S$–LiI/$Li_{5.5}PS_{4.5}Cl_{1.5}$/Li–In battery shows similar variations of resistances of the active material and solid electrolyte interfaces. However, these values are significantly higher than that of the $3Li_2S$–LiI/$Li_{5.5}PS_{4.5}Cl_{1.5}$/Li–In battery during the first cycle due to the increased Li-ion conductivity for the cathode mixture after the introduction of LiI.

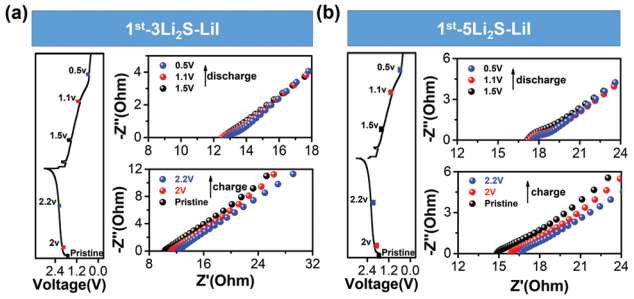

Fig. 4 *In situ* EIS evaluation of $Li_{5.5}PS_{4.5}Cl_{1.5}$-based solid-state Li–S batteries using $3Li_2S$–LiI (a) and $5Li_2S$–LiI (b) cathode mixtures during the first cycle at 0.13 mA cm^{-2} between 0.4 and 3 V *vs.* Li–In at room temperature.

The rate performances of both assembled solid-state batteries were also investigated at room temperature. As shown in Fig. 5, the $3Li_2SLiI$/$Li_{5.5}PS_{4.5}Cl_{1.5}$/Li–In battery delivers higher discharge capacities than $5Li_2S$–LiI/$Li_{5.5}PS_{4.5}Cl_{1.5}$/Li–In at different charge/discharge rates. These batteries display discharge capacities of 1450 and 1250 mA h g^{-1} at 0.064 mA cm^{-2}, 1300 and 950 mA h g^{-1} at 0.13 mA cm^{-2}, 1200 and 880 mA h g^{-1} at 0.16 mA cm^{-2}, 900 and 700 mA h g^{-1} at 0.32 mA cm^{-2}, 700 and 590 mA h g^{-1} at 0.48 mA cm^{-2}, and 1300 and 950 mA h g^{-1} when the C-rate recovers to 0.13 mA cm^{-2}. The former battery exhibits better rate capability and sustainable cyclability than the latter, indicating that $3Li_2S$–LiI possesses superior electrochemical performance than $5Li_2S$–LiI at a room temperature charge/discharge rate.

Furthermore, the effect of operating temperatures on $3Li_2S$–LiI and $5Li_2S$–LiI cathodes was also investigated. We compared

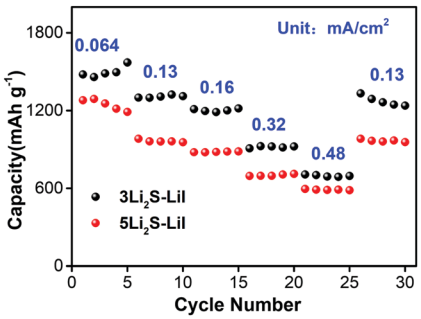

Fig. 5 Rate performance of $3Li_2S$–LiI/$Li_{5.5}PS_{4.5}Cl_{1.5}$/Li–In and $5Li_2S$–LiI/$Li_{5.5}P\ S_{4.5}Cl_{1.5}$/Li–In batteries.

the conductivity of the positive electrode mixture and electrolyte at different temperatures. Fig. 6a shows the ionic conductivity of the $Li_{5.5}PS_{4.5}Cl_{1.5}$ solide electrolyte at 0 °C, room temperature, and 60 °C, respectively. At the same time, we also tested the ionic conductivities of $3Li_2S$–LiI and $5Li_2S$–LiI at 0 °C, RT, and 60 °C, respectively (Fig. 6b). Fig. 6c depicts the 1st and 100th charge/discharge profiles of solid-state batteries using $3Li_2S$–LiI and $5Li_2S$–LiI cathodes cycled at 0.32 mA cm^{-2} at 60 °C. Similar charge/discharge curves and voltage plateaus are observed for both electrodes at high temperatures. $3Li_2S$–LiI delivers an initial discharge capacity of 1600 mA h g^{-1} and retains 600 mA h g^{-1} after 100 cycles. In contrast, $5Li_2S$–LiI shows a lower capacity of 1300 mA h g^{-1} and retains 400 mA h g^{-1} after the same cycling periods (Fig. 6d). Both batteries suffer severe degradation of the discharge capacity during cycling at 60 °C compared to that at 25 °C, due to the intense volume changes at high operating temperatures.[37] Fig. 6e illustrates the charge/discharge plots of $3Li_2S$–LiI and $5Li_2S$–LiI electrodes cycled at 0.32 mA cm^{-2} at 0 °C. Compared to the curves at higher temperatures, a low discharge plateau at 0.6 V *vs.* Li–In disappears for both electrodes. $3Li_2S$–LiI displays a higher initial discharge capacity than $5Li_2S$–LiI (550 mA h g^{-1} *vs.* 350 mA h g^{-1}). Interestingly, both electrodes show a slightly increased discharge capacity during the subsequent cycling in Fig. 6f. After 100 cycles, $3Li_2S$–LiI and $5Li_2S$–LiI exhibit discharge capacities of 700 and 500 mA h g^{-1}, respectively. We also tested with higher current density and longer cycles (Fig. S4, ESI†). As we know, solid-state Li–S batteries significantly suffer

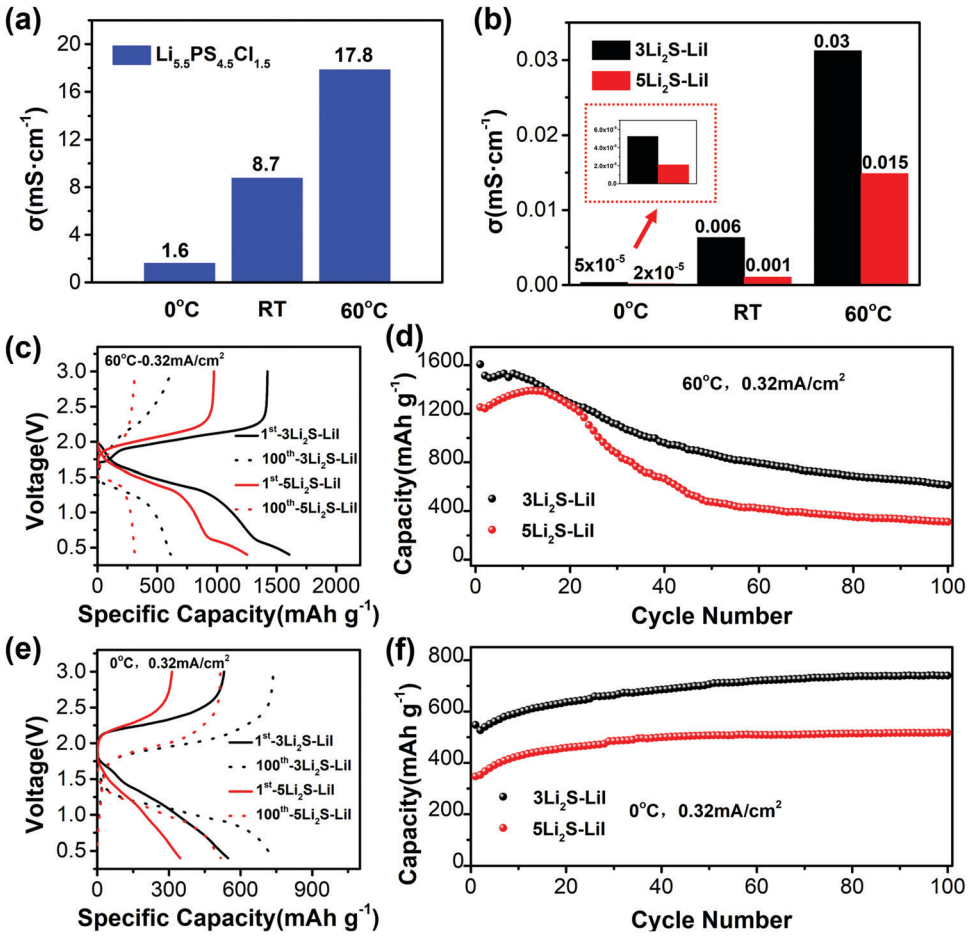

Fig. 6 (a) The ionic conductivity of the $Li_{5.5}PS_{4.5}Cl_{1.5}$ solid electrolyte at room temperature, 0 °C and 60 °C, respectively. (b) The ionic conductivity of $3Li_2S$–LiI and $5Li_2S$–LiI at room temperature, 0 °C and 60 °C, respectively. Charge/discharge profiles (c and d) and cycling performances (e and f) of $Li_{5.5}PS_{4.5}Cl_{1.5}$-based solid-state Li–S batteries using $3Li_2S$–LiI and $5Li_2S$–LiI cathode mixtures cycled at different operating temperatures: 60 °C, and 0 °C, respectively.

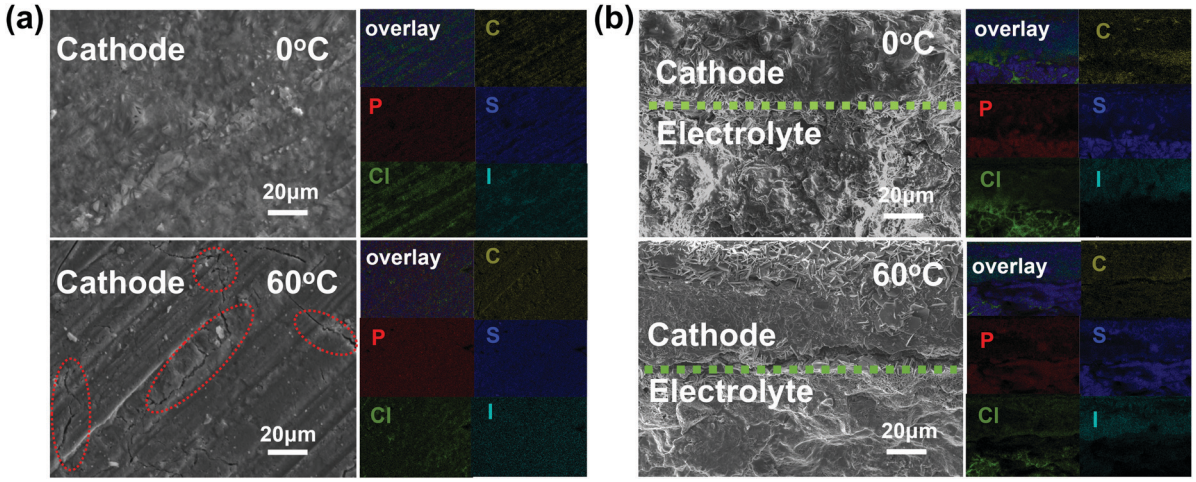

Fig. 7 SEM images and EDX elemental mapping of different sections for $3Li_2S$–LiI/$Li_{5.5}PS_{4.5}Cl_{1.5}$/Li–In solid-state batteries cycled at 0.32 mA cm^{-2} at different temperatures after 100 cycles: (a) surface section and (b) the cross-section of the cathode and solid electrolyte bilayer pellet.

volume changes during cycling, degrading the effective contact between active materials and solid electrolytes. Meanwhile, under freezing ambient conditions, the contraction of the cathode mixture can mitigate the volume variations and provide a better solid/solid contact between Li_2S-based active materials and $Li_{5.5}PS_{4.5}Cl_{1.5}$ solid electrolytes, resulting in superior cycling performances.

To further verify our assumption, SEM images of the surface and cross-section of solid-state batteries after 100 cycles are investigated. As shown in Fig. 7a, the dense surface morphology is observed for the solid-state battery cycled at 0 °C after 100 cycles, while many obvious cracks are observed as depicted with red dotted lines when the battery worked at 60 °C, suggesting that the battery suffers smaller volume variations under the latter condition compared to the former after 100 cycles. Moreover, when the battery was cycled at an elevated temperature after 100 cycles, a large gap is observed between the cathode mixture and the solid electrolyte layer from the cross-section image in Fig. 7b. In comparison, no crack is observed for the cross-section of the low-temperature cycled bilayer pellet. The EDX elemental mapping results also confirm our observations that the solid-state battery cycled at 0 °C possesses a better solid/solid contact than that working at 60 °C after 100 cycles. The poor cycling performances of solid-state batteries at high temperature are associated with the formation of these cracks in the cathode mixture and a significant gap between the cathode and solid electrolyte bilayers.

Conclusions

In this work, the influence of Li-ion conductivity of a Li_2S cathode mixture in the battery performance of solid-state Li–S was carefully investigated. Li_6PS_5Cl is replaced with $Li_{5.5}PS_{4.5}Cl_{1.5}$ electrolyte (8.7 mS cm^{-1} *vs.* 1.1 mS cm^{-1}) to enhance the Li-ion conductivity, resulting in higher discharge capacities and superior capacity retentions with a commercial Li_2S cathode. Moreover, to improve the Li-ion conductivity of commercial Li_2S, the particle size is lowered *via* the mechanical milling process. The corresponding solid-state Li–S batteries using the milled Li_2S cathode and $Li_{5.5}PS_{4.5}Cl_{1.5}$ electrolyte show improved discharge capacities and cyclability compared to those using the commercial Li_2S cathode. In addition, LiI is introduced to further enhance the ionic conductivity of M-Li_2S. The $3Li_2S$–LiI cathode with the highest Li-ion conductivity and a comparable active loading amount displays a high initial discharge capacity of 1190 mA h g^{-1} at 0.32 mA cm^{-2} at room temperature and maintains 770 mA h g^{-1} after 100 cycles with a capacity retention of 64.7%. Furthermore, it also exhibits a higher initial discharge capacity at 60 °C, while suffering from rapid degradation of capacities due to the severe volume variations at elevated temperatures. In contrast, the battery delivers increased discharge capacities with cycling numbers at the beginning and becomes stable during long cycling at 0 °C because of the mitigated volume changes at low temperatures.

Author contributions

All authors discussed the results, contributed to the manuscript writing, and approved its final version. Jia Xie and Chuang Yu supervised the project. Chaochao Wei performed most of the experiments and wrote the paper with support from Jia Xie, Chuang Yu, and Shijie Cheng. Linfeng Peng, Ziqi Zhang, Nuonan Xu, Zhongkai Wu and Cong Liao revised the manuscript and assisted in some parts of the experiments. Wei Zhang and Long Zhang contributed to the data analysis.

Conflicts of interest

There are no conflicts to declare.

Acknowledgements

This work was supported by the National Natural Science Foundation of China (No. 51821005 and 21975087).

We gratefully acknowledge the Analytical and Testing Center of HUST for technical support.

Notes and references

1 C. Zheng, Y. Ruan, J. Su, Z. Song and Z. Wen, *Chem. Eng. J.*, 2021, **411**, 128508.
2 L. Peng, H. Ren, J. Zhang, S. Chen, C. Yu, X. Miao, Z. Zhang, Z. He, M. Yu, L. Zhang, S. Cheng and J. Xie, *Energy Storage Mater.*, 2021, **43**, 53–61.
3 H. T. Ren, Z. Q. Zhang, J. Z. Zhang, L. F. Peng, Z. Y. He, M. Yu, C. Yu, L. Zhang, J. Xie and S. J. Cheng, *Rare Met.*, 2021, **1**, 1–9.
4 M. Wang, X. Xia, Y. Zhong, J. Wu, R. Xu, Z. Yao, D. Wang, W. Tang, X. Wang and J. Tu, *Chem. – Eur. J.*, 2019, **25**, 3710–3725.
5 J. Li, Y. Xu, Y. Zhang, C. He and T. Li, *J. Mater. Chem. A*, 2020, **8**, 19544–19554.
6 R. Zhu, F. Liu, W. Li and Z. Fu, *ChemistrySelect*, 2020, **5**, 9701–9708.
7 D. Song, Z. Xixi, Z. Hongzhou, X. Lianqi and D. Qigao, *J. Mater. Chem. A*, 2019, **7**, 3895–3902.
8 S. Li, W. Zhang, J. Zheng, M. Lv, H. Song and L. Du, *Adv. Energy Mater.*, 2021, **11**, 2000779.
9 S. Wang, X. Xu and X. Zhang, *J. Mater. Chem. A*, 2019, **7**, 18612–18618.
10 A. Mkt, Z. A. Lei, A. Na, B. Rc, A. Mf, Y. A. Le and Y. A. Wen, *Chem. Eng. J.*, 2020, **407**, 127149.
11 H. Yuan, H. Peng, J. Huang and Q. Zhang, *Adv. Mater. Interfaces*, 2019, **6**, 1802046.
12 P. Bonnick, K. Niitani, M. Nose, K. Suto and J. Muldoon, *J. Mater. Chem. A*, 2019, **7**, 24173–24179.
13 S. Xu, C. Y. Kwok, L. Zhou, Z. Zhang, I. Kochetkov and L. F. Nazar, *Adv. Funct. Mater.*, 2020, **31**, 2004239.
14 M. Nagao, A. Hayashi and M. Tatsumisago, *J. Mater. Chem.*, 2012, **22**, 10015–10020.
15 M. Nagao, A. Hayashi and P. M. Tatsumisago, *Energy Technol.*, 2013, **1**, 186–192.
16 B. Yang, C. Yza, C. Wl, A. Lm, C. Yba and B. Gc, *Chem. Eng. J.*, 2020, **396**, 125334.
17 S. Ma, Z. Zhang, Y. Wang, Z. Yu and P. Zuo, *Chem. Eng. J.*, 2021, **418**, 129410.
18 T. Matsuyama, A. Hayashi, T. Ozaki, S. Mori and M. Tatsumisago, *J. Mater. Chem. A*, 2015, **3**, 14142–14147.
19 S. Gu, X. Huang, Q. Wang, J. Jin, Q. Wang, Z. Wen and R. Qian, *Lithium–Sulfur Batteries*, 2017, vol. 5, pp. 13971–13975.
20 S. Passerini, L. Lodovico, S. M. Hosseini and A. Varzi, *Energy Technol.*, 2019, **7**, 1801013.
21 M. Shin and A. A. Gewirth, *Adv. Energy Mater.*, 2019, **9**, 1900931.
22 X. Chen, L. Peng, L. Yuan, R. Zeng, J. Xiang, W. Chen, K. Yuan, J. Chen, Y. Huang and J. Xie, *J. Energy Chem.*, 2019, **37**, 111–116.
23 D. Shao, L. Yang, K. Luo, M. Chen and X. Wang, *Chem. Eng. J.*, 2020, **389**, 124300.
24 C. Yu, S. Ganapathy, E. V. Eck, L. V. Eijck and M. Wagemaker, *J. Mater. Chem. A*, 2017, **5**, 21178–21188.
25 Z. Lin, Z. Liu, N. J. Dudney and C. Liang, *ACS Nano*, 2013, **7**, 2829–2833.
26 C. Yu, S. Ganapathy, J. Hageman, L. van Eijck, E. R. H. van Eck, L. Zhang, T. Schwietert, S. Basak, E. M. Kelder and M. Wagemaker, *ACS Appl. Mater. Interfaces*, 2018, **10**, 33296–33306.
27 S. Motoshi, K. Atsutaka, S. Atsushi, H. Akitoshi and T. Masahiro, *Electrochim. Acta*, 2018, **286**, 158–162.
28 T. Hakari, A. Hayashi and M. Tatsumisago, *Adv. Sustainable Syst.*, 2017, **1**, 1700017.
29 Z. Zhang, J. Zhang, H. Jia, L. Peng, T. An and J. Xie, *J. Power Sources*, 2020, **450**, 227601.
30 C. Wei, C. Yu, Z. Wu, L. Peng, S. Chen and J. Xie, *Energy Storage Sci. Technol.*, 2021, 1–15, DOI: 10.19799/j.cnki.2095-4239.2021.0513.
31 X. Sun, J. Liang, S. Qian, Z. Yang and H. Huang, *J. Mater. Chem. A*, 2018, **6**, 23712–23719.
32 B. Zza, A. Jz, B. Hja, C. Lpa, A. Tao and X. A. Jia, *J. Power Sources*, 2020, **450**, 227601.
33 R. C. Xu, X. H. Xia and S. H. Li, *J. Mater. Chem. A*, 2017, **5**, 6310–6317.
34 Z. Zhang, J. Zhang and Y. Sun, *J. Energy Chem.*, 2020, **41**, 171–176.
35 R. P. Rao and M. Seshasayee, *J. Non-Cryst. Solids*, 2006, **352**, 3310–3314.
36 C. Yu, J. Hageman, S. Ganapathy, L. V. Eijck, L. Zhang, K. Adair, X. Sun and M. Wagemaker, *J. Mater. Chem. A*, 2019, **7**, 10412–10421.
37 H. Yan, H. Wang, D. Wang, X. Li, Z. Gong and Y. Yang, *Nano Lett.*, 2019, **19**, 3280–3287.